2020-01-13

Quantifying the Impact of Nonlinear Internal Waves on the Marine Atmospheric Surface Layer

Ortiz-Suslow, David G.; Wang, Qing; Kalogiros, John; Yamaguchi, Ryan; Celona, Sean; Paolo, Tony de; Terrill, Eric; Shearman, R. Kipp; Welch, Pat

IEEE

D. G. Ortiz-Suslow et al., "Quantifying the Impact of Nonlinear Internal Waves on the Marine Atmospheric Surface Layer," 2019 IEEE/OES Twelfth Current, Waves and Turbulence Measurement (CWTM), San Diego, CA, USA, 2019, pp. 1-9.
http://hdl.handle.net/10945/66925

Quantifying the Impact of Nonlinear Internal Waves on the Marine Atmospheric Surface Layer

1st David G. Ortiz-Suslow
Naval Postgraduate School
Monterey, USA
dortizsu@nps.edu

2nd Qing Wang
Naval Postgraduate School
Monterey, USA
qwang@nps.edu

3rd John Kalogiros*
Naval Postgraduate School
Monterey, USA
jkalog@noa.gr

4th Ryan Yamaguchi
Naval Postgraduate School
Monterey, USA
ryamaguch@nps.edu

5th Sean Celona
Scripps Institution of Oceanography
La Jolla, USA
scelona@ucsd.edu

6th Tony de Paolo
Scripps Institution of Oceanography
La Jolla, USA
adepaolo@ucsd.edu

7th Eric Terrill
Scripps Institution of Oceanography
La Jolla, USA
email address

8th R. Kipp Shearman
Oregon State University
Corvallis, OR
shearman@coas.oregonstate.edu

9th Pat Welch
Oregon State University
Corvallis, OR
tpw@coas.oregonstate.edu

10th Ivan Savelyev
U.S. Naval Research Laboratory
Washington D.C., USA
ivan.savelyev@nrl.navy.mil

***Abstract*—In the coastal environment, the oceanic flow over varying bathymetry can displace the isopycnal surfaces and, thus, generate nonlinear internal waves. These high frequency waves can propagate across large distances and over their lifetime significantly influence local currents and turbulence within a coastal region. These waves also create a common phenomenon that is recognized by even a casual observer: smooth, quasilinear bands of water that disrupt the typically rippled sea surface. While NIWs are an important oceanic process and their surface expression has been characterized and discussed for decades, investigators have not linked the presence of internal wave-driven surface roughness to an atmospheric response. Here we use a combination of oceanic and atmospheric measurements, as well as ocean surface visualization, to show that NIWs can alter the flow within the MASL and the subsequent momentum flux across the air-sea interface, at the dominant temporal-spatial scales of the NIWs. Our measurements were collected from the FLIP, which was deployed as part of the Coupled Air Sea Processes and Electromagnetic ducting Research (CASPER) West Coast field campaign. Using a thermistor chain, X band marine radar, upward- and downward-looking ADCP, as well as a visual field camera imaging the ocean surface near *FLIP*, we were able to identify several NIW events and track individual waves incident to the platform. This information was used to isolate the atmospheric response, as captured by a profile of meteorological flux sensors installed on a mast that was deployed from *FLIP*'s boom. The observed NIW-interactions were found in multiple cases with different MASL conditions and internal wave properties. In the context of CASPER, the surface roughness associated with NIWs represents a persistent, quasi-Lagrangian heterogeneity that may impact the atmospheric gradients, which in turn modulates the index of refraction and the propagation of electromagnetic radiation.**

Funding provided by Office of Naval Research N0001418WX01087.

*Other Affiliation: National Observatory of Athens, Athens, GR

***Index Terms*—Nonlinear Internal Waves, Marine Atmospheric Surface Layer, Air-Sea Interaction, Field Observations**

I. Introduction

The ocean surface roughness is held primarily by the short gravity and capillary waves that are widely distributed across the air-sea interface. These small waves, or ripples, respond quickly to changes in the local environment and are both indicative of and the basis for the mechanical interaction between the atmosphere and ocean. In fact, it has long been recognized that the apparent *roughness* of a water body's surface is directly related to the tangential wind stress applied to that surface [1]. The abstract concept of ocean surface roughness, z_0, is related, in some way, to the physical wave scales. This is analogous to the concept of a significant wave height (H_s), which is a wholly statistical quantity, that is representative of the physical dimension of the local wave field. Therefore, it has been one of the goals of air-sea interaction study to develop parameterizations relating wind speed, forcing (i.e. stress), and wave statistics to z_0 for a wide variety of conditions, and, in turn, relate z_0 to the cumulative air-sea interaction parameter: the aerodynamic drag coefficient, C_D [2]–[7]. The drag coefficient remains the primary means for predicting the interfacial flux of momentum and energy (analogous coefficients for sensible and latent heat flux) for a given environmental state in both obervationally- and numerically-based studies. Thus, developing a more complete understanding of C_D variance is critical to better and more accurate modeling of atmosphere-ocean coupled processes. The short waves on the ocean surface are forced by the wind, but they can also be driven by hydrodynamics. For example, longer surface gravity waves are known to force these short

978-1-5386-5485-9/19/$31.00 ©2019 IEEE

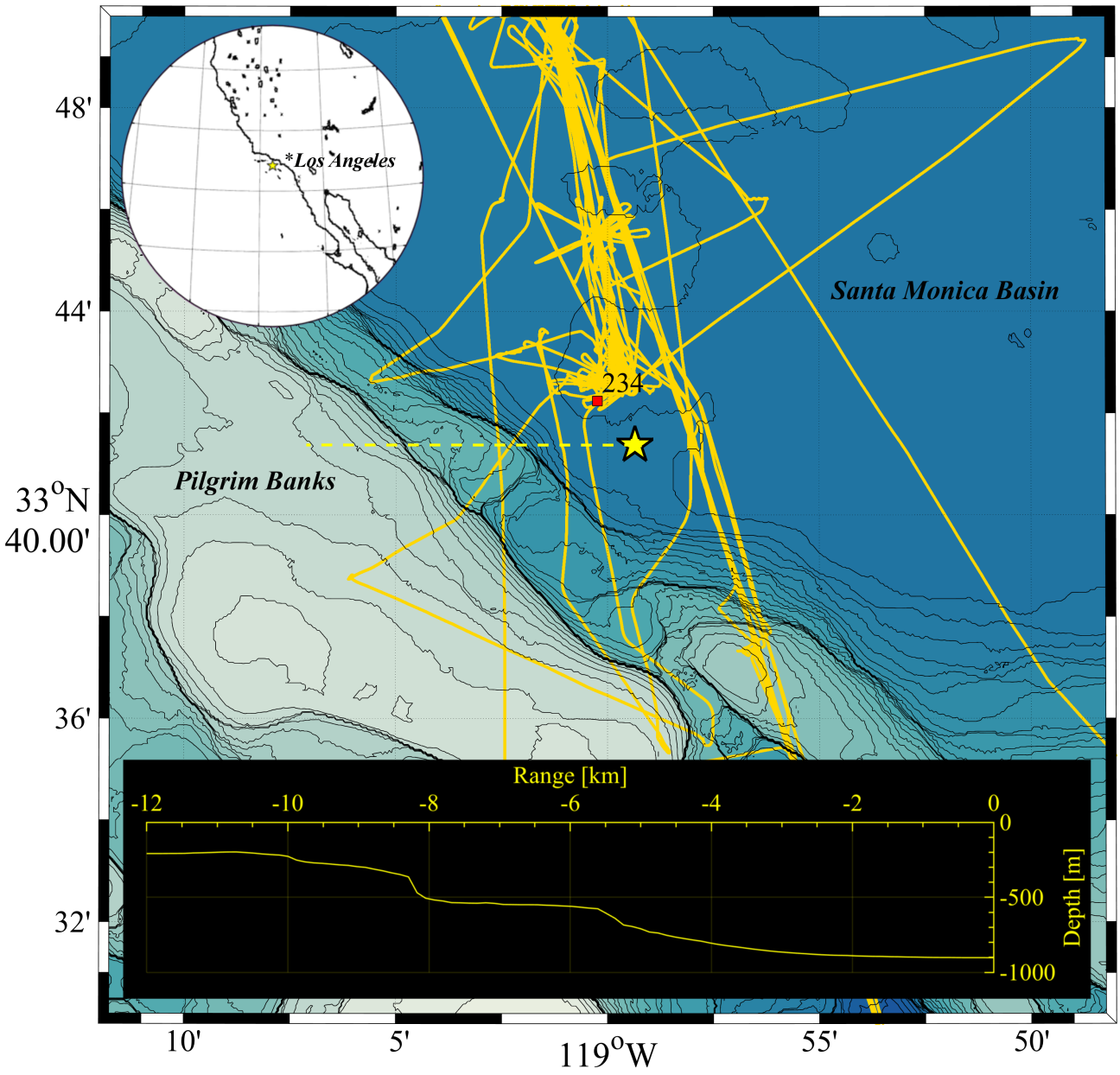

Fig. 1: The CASPER-West field study location, focused on the location of *FLIP* (yellow star). The nearby CDIP 234 buoy is marked, as well as the *Sally Ride* GPS track. The depth across Pilgrim Banks due west of *FLIP* is shown, which is the supposed generation point of many of the NIWs observed for this study. Depth contours are in meters and the topographic data source is [8].

waves through the hydrodynamic modulation by the periodic, orbital velocity of the carrier wave [9]. In addition, larger scale oceanic internal waves have been known for decades to modulate the apparent roughness of the ocean surface [10], much through the same process as observed for surface waves, but on a larger scale [11].

Nonlinear internal waves (NIWs) are ubiquitous features of the coastal environment that are readily visible by even casual observers, and can be identified as bands of smooth water, or slicks, propagating slowly across the surface. Their prevalence in coastal waters is due to their primary generation mechanism via the interaction of flow (e.g. tidal) with rapidly changing bathymetry perturbing the isopycnal surfaces. This mechanism results in their largest amplitude response being at the thermocline or mix layer depth, i.e. the largest upper ocean density difference. In the literature, the surface expressions of NIWs have been observed and studied for nearly eight decades [12], [13], but the advent of radar-based satellite imagery greatly expanded the documentation of these phenomena across various coastal settings [14], [15]. NIWs are an important oceanic process in that they can enhance turbulence and transport in coastal areas [16], [17] and their impact can be distributed over

large regions as they propagate and eventually break. While their surface expression clearly shows an impact on the ocean surface roughness, the link between these common ocean features and atmospheric variability has not been established. This gap may be attributed to the need for a confluence of meteorological and oceanographic measurements, in an area with regular NIW activity, to diagnose and analyze the impact NIW have on the marine atmospheric surface layer (MASL).

The Coupled Air Sea Processes and Electromagnetic ducting Research West Coast (CASPER-West) field campaign, in September-October 2017, was a comprehensive air-sea interaction study set to characterize upper ocean and marine atmospheric boundary layer (MABL) variability across a ∼75 km stretch of Southern California coastal ocean. As part of this campaign, the Research Platform *FLIP* was deployed within the Southern California Bight in a region with high NIW activity and a suite of instrumentation capable of observing and analyzing these waves as they propagated near the platform. The present study seeks to address this fundamental question: do NIWs drive turbulent and mean (or bulk) variability within the MASL? Presented here are details on the various techniques used to observe and characterize NIWs and preliminary findings of NIW-atmosphere interaction. The implications of the present findings and the aims of on-going and future work will also be discussed.

II. Field Study and Measurements

A. CASPER-West background

CASPER-West took place within the Southern California Bight and had an observing period September 27 through October 25, 2017 (Fig. 1). The goal of CASPER-West was to characterize the environmental affects on the electromagnetic (EM) propagation from Pt. Mugu along a transect, bearing south-southeasterly across the Santa Monica Basin, ending just offshore of the Santa Cruz-Catalina Ridge (not shown in Fig. 1). In the atmosphere, EM propagation is controlled by the (modified) index of refraction, which in turn, depends on the vertical structure of pressure, temperature, and water vapor content, with the latter having a dominant affect, as well as range (horizontal distance across the Earth's curving surface). Therefore, any process that impacts the vertical gradients within the MABL in an unpredictable manner, will divert the expected radiation path. Typically, in propagation models Monin-Obukhov Similarity Theory (MOST) [18] is used to predict gradients in the atmosphere. Therefore, these propagation models are dependent on the infallibility of this foundational theory. Recent observations have shown that MOST may break-down in certain wave regimes [19] and in the marine to terrestrial boundary layer transition [20]. CASPER was focused on providing the observations necessary to further explore the regimes where MOST breaks-down and if the parameterizations could be adjusted to account for this process. For a more detailed summary of the aims, scope, and work done as part of CASPER, the reader is directed to the article by Wang et al. [21].

The major platforms utilized for CASPER-West were the R/V *Sally Ride* and *FLIP*, which provided a stationary over-the-ocean measurement platform as a corollary to the shore station at Pt. Mugu (∼50 km to the north-northwest). In addition to these large platforms, various autonomous profiling and surface gliders were used to provide more detailed, quasi-Lagrangian measurements of oceanic, as well as, in one case, atmospheric data very close to the interface. Also, several flights were conducted by the Center for Interdisciplinary Remotely Piloted Aircraft Studies (CIRPAS) Twin Otter research aircraft. All of this dynamic sampling was complimented by a suite of NDBC/CDIP wave and meteorological buoys moored in the vicinity.

B. FLIP measurements

This paper focuses on measurements made from *FLIP*. The meteorological data comes from a ∼13 m tall air-sea interaction mast (ASIM) installed at the end of *FLIP*'s port boom (see Fig. 2). The ASIM mast was equipped with overlapping bulk and turbulence-resolving profiles. Here, bulk refers to the slow-varying (∼15-30 minute) wind speed, air temperature, and relative humidity. For the atmospheric turbulence measurements, a vertical array of (7) three-dimensional sonic anemometers and (6) co-located fast-sampling hygrometers enabled using the eddy covariance technique to directly resolve the flux of momentum, sensible (from sonic temperature), and latent heat from 3 to 16 m above the mean water level (MWL; the lowest level on the ASIM mast did not resolve the latent heat flux, the lowest level for this profile was ∼4.5 m above MWL). In addition, two radiometric sea surface temperature (SST) sensors, a boom-tethered, surface-following meteorological mast, and a laser wave gauge (LWG) were deployed from the port boom (Fig 2). One of the radiometric sensors was an RMRCO ROSR[1] system, which is a self-contained measurement package that *in situ* calibrates the observed SST. However, this sensor failed early in the experiment and therefore a post-processing method was used to blend the two radiometers (the other being a fast-response IR pyrometer) and account for reflected downwelling irradiance on the uncalibrated sensor. The details on the processing and quality control of the meteorological sensors deployed from *FLIP*'s port boom are provided in Ortiz-Suslow et al. [22]. A Campbell Scientific Field Camera and ocean temperature string were deployed from the face boom of *FLIP* (Fig. 2). The camera was mounted on a pole (1.39 m above the deck) approximately two thirds of the way along the boom. The camera was oriented to be looking across *FLIP*'s face towards the port boom and the ASIM mast (approximately 76° CCW from the keel). The camera was operated continuously (IR LEDs were used for nighttime capture) from 10/07 through 10/23. Low resolution (640 x 480) images were captured every minute, while a higher resolution (2600 x 1900) image was taken every 10 minutes. However, in IR-mode, the features of the ocean surface could not be visualized.

[1] www.rmrco.com

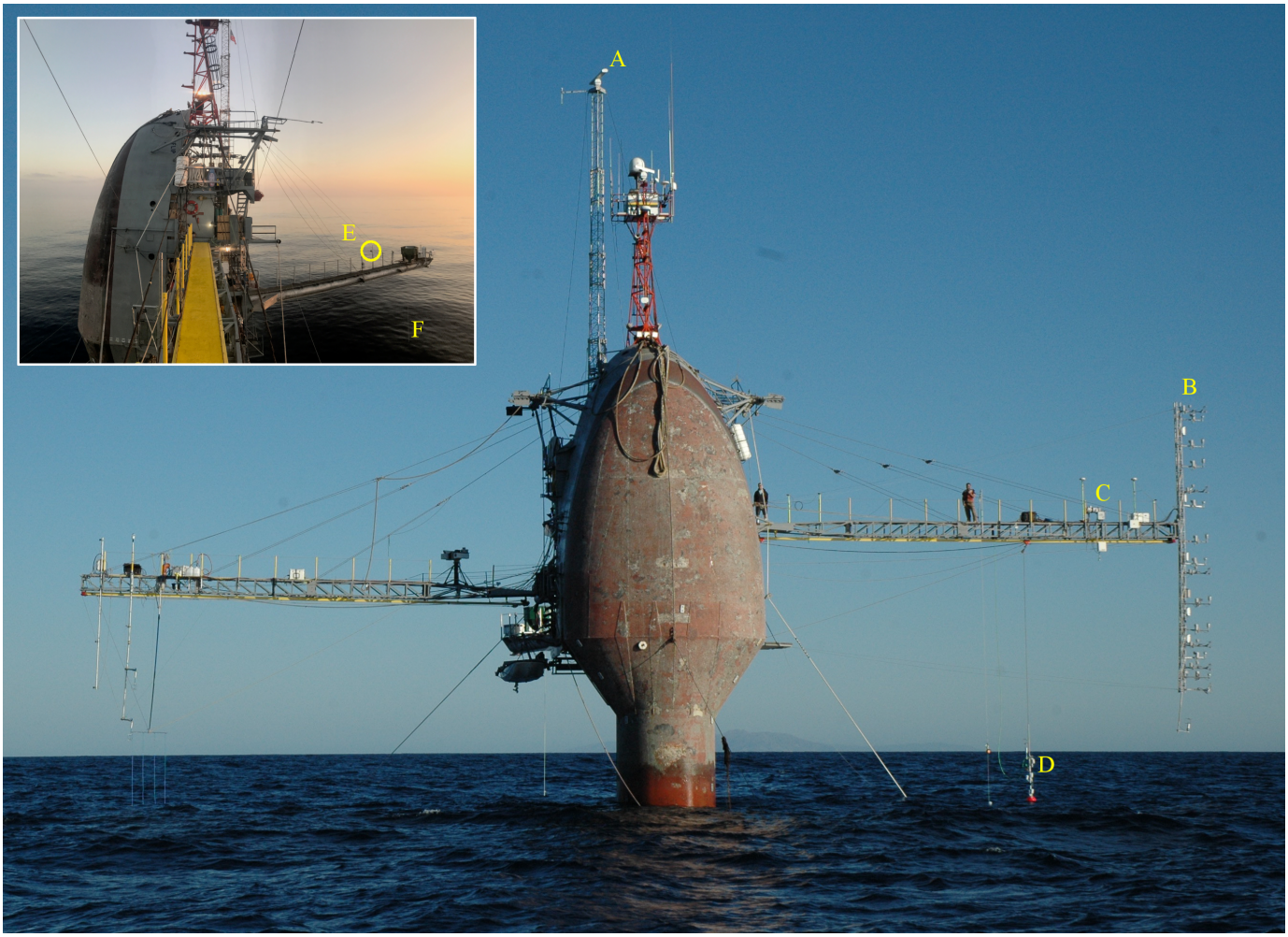

Fig. 2: View of *FLIP* during CASPER-West. (Background) A view from the keel-side with (A) the marine radar used for NIW detections; (B) ASIM mast on portside boom; (C) radiometric sea surface temperature sensors; and (D) *FLIP*'s lowest observing platform (FLOP), a surface-following meteorological mast buoy. Inset: (E) location of field camera used for surface visualization, the field of view was centered on the ASIM mast and (F) location of temperature string tether to the face boom. ADCP's were mounted on the face-side, along the spar on a frame ∼15 m below the surface and that extended out a few meters from the hull.

The temperature string was tethered from the face boom and comprised of 20 temperature sensors spaced approximately every 2 m. A lead plumb weight was attached to the end of the string and the pressure-depth was recorded at one location at the base of the string. The data was recorded on individual sensor's memory cards and downloaded at the end of the experiment. Assuming an approximately linear string, the absolute depth below MWL for each sensor was determined using the geometry of *FLIP*, the inertial motion data from the platform's data acquisition system, and a forced pendulum model. *FLIP* is fairly stationary, but does respond to currents and wave forcing. Detailed analysis of the platform's motion during CASPER-West is included in the Ortiz-Suslow et al. report.

A standard marine X-band radar (MXR) was installed on *FLIP* operating at 9410 +/- 30 MHz with a 1.5s rotational rate, 3km range, 7.5m range resolution, and 1/10° angular resolution for 9/25 through 10/25. This non-coherent radar transmits microwave pulses that interact with small-scale capillary waves to produce images of the ocean surface that are dominated by surface gravity waves. The MXR was mounted at the top of a telescoping mast installed on the upper deck of *FLIP* (Fig. 2).

III. Characterizing NIW from *FLIP*

The presence of smooth bands on the surface of the ocean was immediately evident from the beginning stages of CASPER-West, during the set-up phase. A class of band was visually identified as exhibiting smooth fronts, with a cross-frontal span ∼10 m, propagating with a regular band-to-band separation ∼200 m. These bands were observed most days of the campaign. Using both visual and *FLIP* observations they were linked to NIW activity, most likely generated by tidal flow interacting with local topography (e.g. Pilgrim Banks). It was necessary to establish what mechanism was driving these bands, since other hydrodynamic processes can exhibit similar surface expressions and cause roughness variability, but the

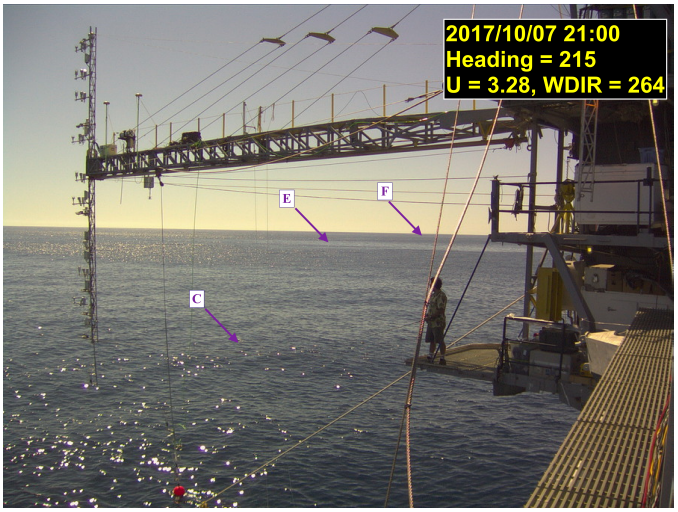

Fig. 3: Sample image of high resolution capture from field camera, wind speed (U) and direction ($WDIR$) given from ∼5 m above MWL. Heading refers to the estimated look direction of the field camera. The location of individual smooth bands (C, E, and F) are marked (see below for details), band D was very thin and only visible closer to the ASIM mast.

TABLE I: Events when NIW were identified from the field camera on *FLIP*.

Date[a]	Start	Stop	MSL[b][m]	*Notes*
10/07	20:30	23:00	0.469↓	Very clear, from SW.
10/08	20:00	01:00	0.718↓	Ends 10/09, from W.
10/10	14:00	20:30	-0.13↑	SSW-SW, confused early.
10/12	15:00	19:50	0.108↓	From SW, very wide.
10/13	13:30	21:00	0.405↓	From SW, wind E then SW.
10/14	15:00	22:10	0.481↓	Faint and thin, SSW-SW.
10/15	14:00	21:30	0.644↑	From SSW, clear 17:10.
10/16	00:00	03:00	0.411↑	Faint, during sea breeze.
10/16	18:00	20:00	0.147↓	Thin, from WSW.
10/19	19:40	20:30	0.006↓	Faint, possibly visible.

[a] Dates/times in UTC, start/stop of when NIW visible in camera.
[b] Mean Sea Level datum, observations from NDBC 9410840, arrow indicates direction of change at $Start$.

atmospheric response to these features may be characteristically different. For example, submesoscale currents can create filament-like frontal structures that could appear very similar to these smooth bands, and which have been documented in the Southern California Bight region [23]. These filaments appear to meander and their spacing is less regular, which helped to distinguish them from the NIW fronts. While also an interesting phenomena, these filament structures were not included in this analysis.

Herein, the phrases smooth band, NIW band, and NIW front will be used interchangeably to refer to the visually-identified smooth band of water associated with NIW activity at the MLD.

A. *Surface Visualization*

Table I summarizes the instances when NIW bands were observable from the field camera. These bands were observed 9 out of the 15 days the camera was in operation. For two of those days, the mean wind speed (U) was >5 m/s and in these conditions it is not possible to discern the bands due to the more dominant windsea development. Excluding these two days, there was an 69.2% incidence rate of NIWs bands near *FLIP* during CASPER-West. The camera footage was reviewed post-experiment (by Ortiz-Suslow) to determine if the bands were present and other characteristics of these features. An example of this footage is provided in Fig. 3. Based on the imagery, band arrival will be judged as when the leading edge of the smooth front reaches the base of the ASIM mast, while band departure corresponds to the arrival of the trailing edge.

Surface visualization was also provided by the MXR. The raw backscatter maps can be averaged (e.g. over 1 minute) to filter out the signal from surface gravity waves. This technique was used to enhance the backscatter associated with lower frequency variability, for example NIW. Fig. 4 provides an example of MXR-visualized NIW from an earlier period than Fig. 3. The bands visible in MXR are narrow rough bands separated by wide smooth areas (i.e. reduced/no backscatter). This differs from the visual identification of the NIW fronts, which typically are associated with narrow smooth bands separated by rough, or rippled, water surface. This highlights that these two visualization techniques observe different components of the same process. The example in Fig. 4 comes from very intense NIW activity, but the field camera was not operating at this time—also these occurred during local night time and easterly winds. During the analysis, the features visible in the MXR from the same time as the camera image in Fig. 3 were matched up with the visual features in the imagery.

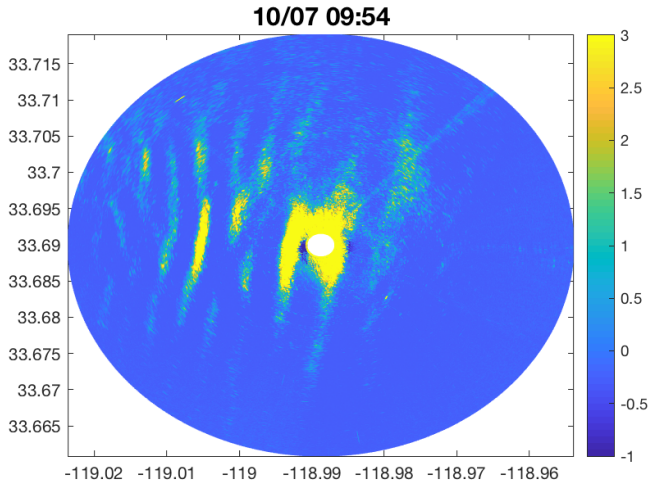

Fig. 4: MXR 60-second averaged image showing NIW fronts propagating from WSW. Color indicates normalized backscatter intensity, bright indicates more backscatter (i.e., rougher).

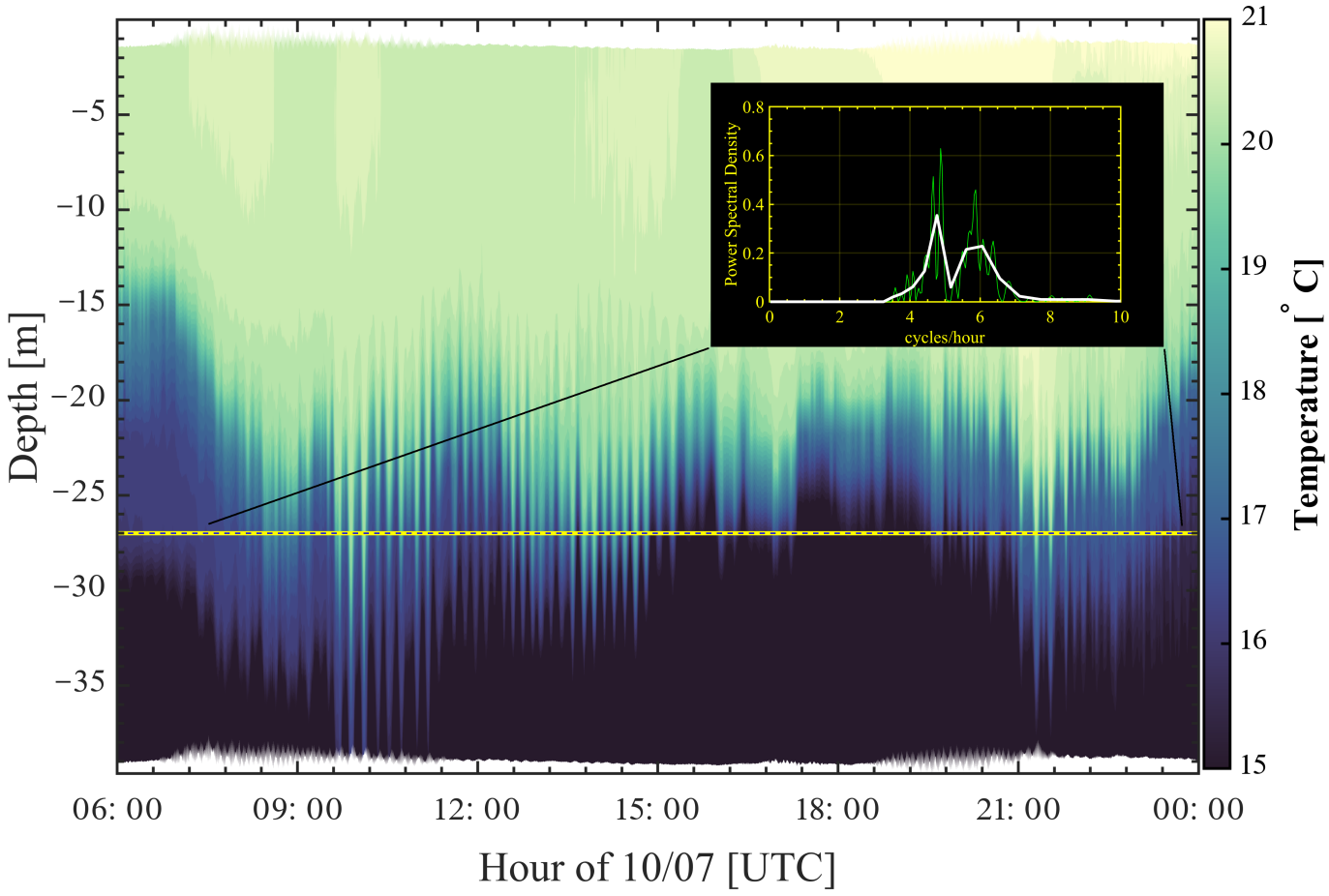

Fig. 5: Temperature contours for Oct. 7 from the *FLIP* temperature string. NIW appear most clearly as depressions/elevations of the isothermals at the MLD and within the transition zone. A spectral decomposition (full (green) and smoothed (white) resolutions) is given for the depth -27 m.

B. Ocean Measurements

FLIP's temperature string was used to link the NIW-driven variability within the ocean, to the appearance of the surface bands both in the field camera and MXR. The tilt-corrected temperature-depth readings were sampled at 2 Hz and sub-sampled to 30 seconds and re-interpolated (linear) at a 0.5 m vertical resolution. The temperature structure revealed a MLD between 15 and 25 m below the surface, with a transition zone 5-10 m wide. The relatively short length of the string meant that occasionally the measurements did not extend beyond the MLD and transition zone. The most intense NIW activity occurred at the MLD, with an example from Oct. 7 given in Fig. 5. From this case, it is possible to see large oscillations at the MLD corresponding with the time of Fig. 4. Later in the day, another, less intense NIW event occurred (approximately 20:30 to 23:30), which corresponds to the field camera imagery in Fig. 3. Spectral analysis of the bandpass-filtered (cut-offs 5 and 17 minutes) temperature signal at $z{=}{-}27$ m revealed two distinct peaks at 4.7 and 6.06 cycles per hour, or approximately 13 and 10 minutes, respectively. The lower frequency peak was associated with the later, less intense event.

IV. NIW-Atmosphere Interactions

The characteristics of quasi-linear, regularly spaced bands propagating across the coastal ocean with no particular dependence on wind speed or direction would be indicative of NIW. The signals apparent in the temperature structure (Fig. 5) are evidence that NIW were active during CASPER-West. The timing of the individual surface bands (Table I) were synced with the temperature variability to establish that the these bands were due to NIW. October 7 provides an excellent example of favorable wind conditions and strong NIW activity for this analysis.

From 20:30 to 23:00 UTC, several distinct bands were observed propagating past *FLIP*, with 7 major arrivals noted in the field camera imagery (Fig. 6). A *major* arrivals indicates that the band was obvious in the imagery and could be tracked through successive frames as it propagated towards *FLIP*. These bands propagated relatively slowly ($\sim$10 cm/s) and were $\sim$10 m wide, so their individual arrival time of the leading edge relative to the ASIM mast could be accurately estimated via inspection (corresponding departure time as well). These times corresponded with maximum/minimum temperature anomalies at the MLD, i.e. peaks and troughs

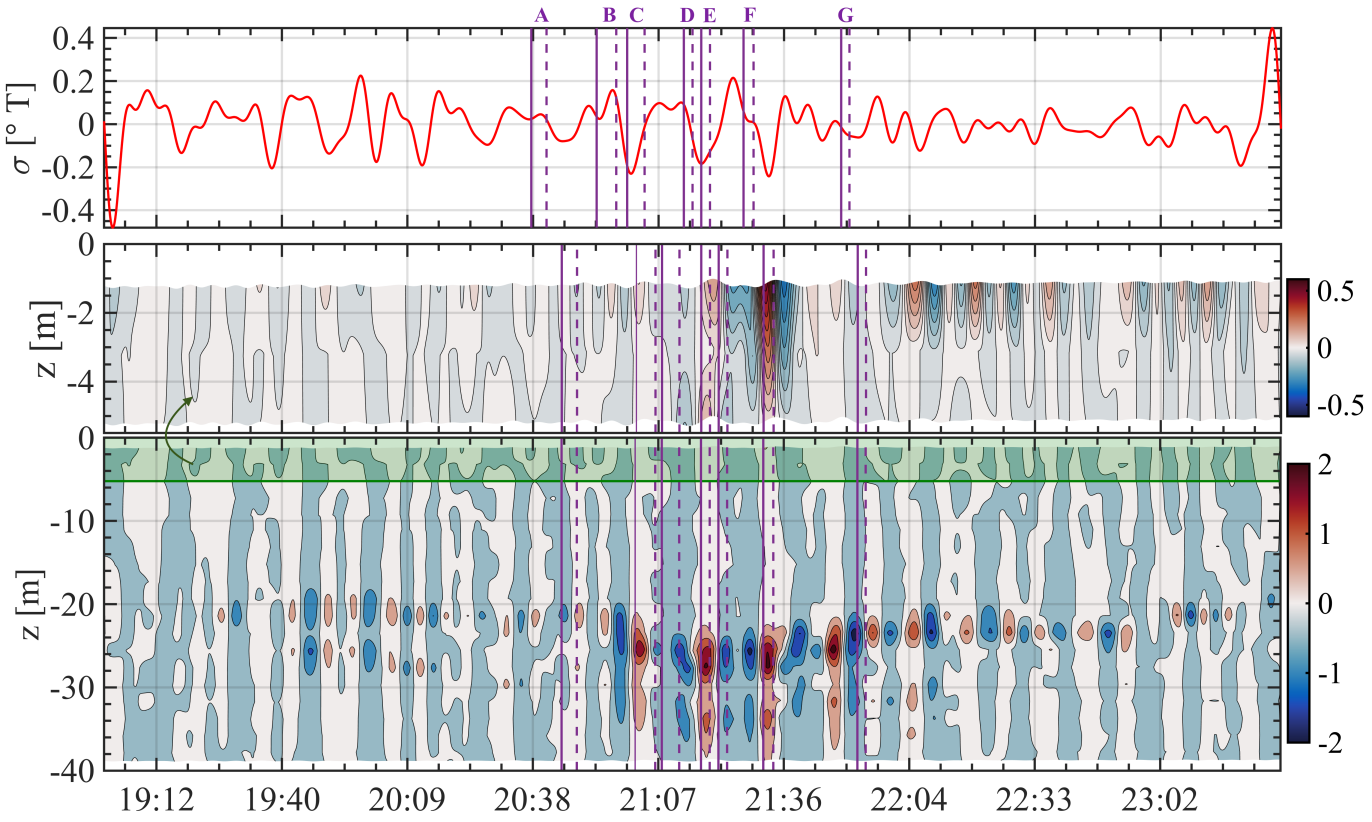

Fig. 6: Temperature anomaly for skin temperature (top), upper 5 m of temperature string (middle), and full 40 m column (lower). Anomaly was defined as the detrended (over entire period), bandpass filtered temperature in Celsius (cut-offs at 17 and 5 minutes). A-G mark individual band arrivals and the time-shift between the skin and ocean temperature is an estimate of the signal lag due to the spatial separation of the two observation points. This was calculated assuming a 10-m wide band and a 20-m wide separation. Solid and dashed lines mark arrival and departure of leading and trailing edges, respectively.

of individual NIWs (Fig. 6). Here, temperature anomaly is the bandpass filtered time series that was detrended over the analysis window (Fig. 6 has a window ∼4.5 hours long).

While not every NIW corresponded to a surface band, it would appear as if the stronger waves were able to generate this phase-locked surface expression. Theoretically, for a monochromatic internal wave propagating along the MLD, one would expect the smooth band at the divergence of NIW-drive surface velocities, which occur twice per wave length [11]. For this case, the real conditions correspond well to the theoretical expectations. The smooth band is easier to discern, visually, since it stands out relative to the already rippled surface, which contains short waves from wind and NIW forcing.

Interestingly, during this time (20:30 to 23:00 UTC) the mean horizontal current changes from being eastward to westward directions, indicating a change in tide from flood to ebb. This was observed in the upward-looking ADCP deployed from *FLIP*, which captured the upper 15 m of the water column. This would cause a sign reversal in the Doppler effect on the NIW (propagating eastward) over this period. This current reversal coincided with the arrival/departure of G, after which a series of thinner and higher frequency surface bands could be seen propagating from the west, in the field camera images. These arrivals were thinner and harder to discern due to an increase in windsea and sun glint that made band-identification challenging. However, this observation would follow from some NIW-current interaction, which would impact the NIW-atmosphere interactions by altering the band characteristics. The presence of more wind waves made MXR retrieval difficult to interpret, even with the 1-minute averaging. Due to these challenges, these thinner bands were not included in the air-sea interaction analysis. An example from 10/12 (16:00 to 18:00 UTC) of the atmospheric response to a single propagating smooth band is given in Fig. 7. During this case, the bands are lower frequency (longer spacing between successive smooth bands) than those identified on 10/7. Also, during this period the mean wind speed was ∼2 m/s, which is very low in terms of conventional wind forcing models or parameterizations. While in both cases, NIW were observed at the MLD, they were not only different frequencies, but the perturbations were less symmetrical on 10/12, appearing as elevation waves. Furthermore, the MXR did not register any surface signature and these were only visible in the field camera. This suggests that the properties of the NIW are key to the actual surface wave bandwidth excited by this forcing. The relatively low frequency and wide spacing between bands allowed for a more detailed analysis of the quasi-instantaneous profile response of the MASL.

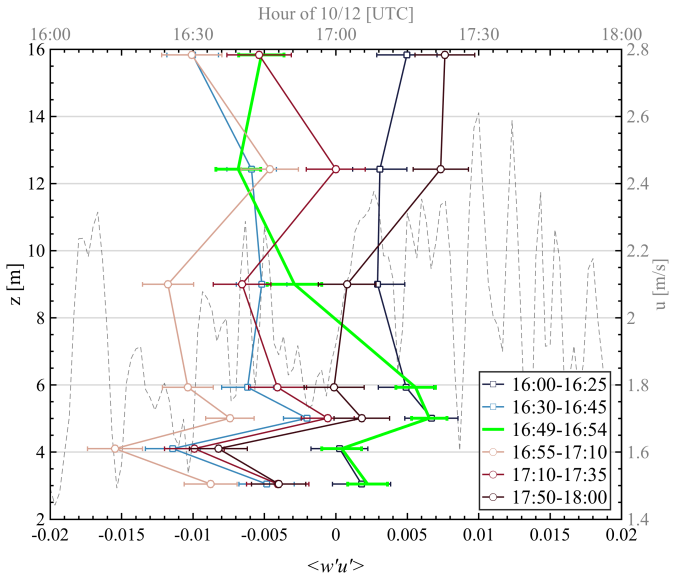

Fig. 7: Profiles of the mean stream-wise covariance (averaging window given) between 16:00 - 18:00 UTC on 10/12. The green profile marks the time when the NIW band was at the *FLIP* ASIM mast. The grey dashed line gives the along-stream velocity time series (grey axis). For the covariance and wind velocity, a 120 second bin-average was used with 50% overlap. The $<w'u'>$ represent means $\pm$ 95% confidence intervals over the time period given.

The stream-wise covariance between the along-(u) and vertical-(w) wind ($<w'u'>$), is the primary component of the Reynolds stress, which under typical MASL conditions makes up the entire tangential stress by the wind on the ocean surface. In this convention, $<w'u'>>0$ indicates upward momentum flux[2]. The profiles in Fig. 7 reveal that a systematic transition occurs for the turbulence in the MASL, as the band approaches *FLIP*, with a distinct $\partial<w'u'>/\partial z$, when the band arrives. On the upwind side of the front, the profile slowly returns back to the pre-arrival condition. This response-relaxation cycle occurs on top of underlying profile variability that was not due to the NIW. Furthermore, this response was not explained by changes in the mean u over this period.

From the ocean temperature structure from -40 m to the skin surface, NIW-driven signals are evident through much of the mixing layer (e.g., Fig. 6), but there was little correlation between the mixing layer variability up to the skin surface. This suggests that the intense mixing in the upper 1-2 m wipes out any residual thermal signature from the NIW. Therefore, in these cases, NIW were not expected to impact the atmospheric scalar structure (temperature and humidity), but would be expected to impact the inertia and momentum flux within the MASL due to the flow adjustment from rough-smooth. This is evident in Fig. 7 and was also observed for 10/7 (not shown here).

[2]In a mean sense, the air-sea momentum flux should always be downward (<0), but under short averaging windows, low winds, and/or certain wave states, upward momentum flux is possible and expected.

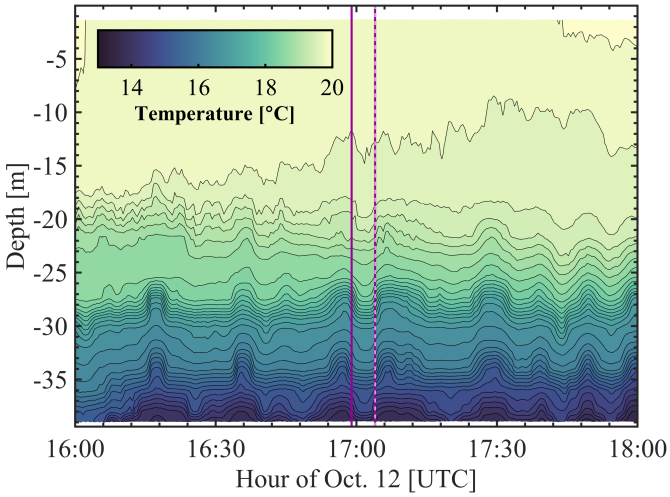

Fig. 8: Temperature contours (not anomalies) for 10/12 16:00 to 18:00 UTC. The internal waves can be seen at approximately -27 and -35 m. The arrival (solid) and departure (checkered) times of the surface band analyzed in Fig. 7 are marked.

V. Summary

A suite of oceanographic and atmospheric observing systems installed on *FLIP* during CASPER-West have been used to investigate the interactions between NIW and the MASL. This article has focused on how these systems were used to identify NIWs and highlighted two cases where NIW were observed and linked with surface roughness, as well as atmospheric, variability. Preliminary results suggest that NIW do exert a mechanical forcing on the MASL, through the flow adjustment across the smooth-rough regions of the surface, which are caused by the presence of NIWs. However, no clear link was made between the NIWs and mean or turbulent flux scalar variability. This study represents one of the first focused investigations into the physical interactions between NIWs and the atmosphere. Future work will seek to understand the net impact NIWs have on the atmospheric variability and the exact mechanism for this interaction. Understanding the physical coupling more precisely will help with modeling this as a source MASL wind speed and momentum flux variability over coastal waters.

Acknowledgment

This work was funded by ONR N0001418WX01087. The authors would like to thank the Captain and crew of the *FLIP* for their tremendous efforts in helping facilitate this work. The authors would like to recognize members of the NPS Boundary Layer Processes group who helped with experiment preparation and data collection: Denny Alappattu, Richard Lind, Alex Olson, Ben Wauer, Kyle Franklin, and Anna Hook.

References

[1] H. Charnock, "Wind Stress on a Water Surface," *Quarterly Journal of the Royal Meteorological Society*, vol. 81, no. 350, p. 1, 1955.

[2] S. D. Smith, "Wind Stress and Heat Flux over the Ocean in Gale Force Winds," *Journal of Physical Oceanography*, vol. 10, p. 18, 1980.

[3] W. Large and S. Pond, "Open Ocean Momentum Flux Measurements in Moderate to Strong Winds," *Journal of Physical Oceanography*, vol. 11, p. 13, 1981.

[4] C. W. Fairall, A. A. Grachev, A. J. Bedard, R. T. Nishiyama, M. K. Secretary, D. J. Baker, and J. L. Rasmussen, "NOAA Technical Memorandum ERL ETL-268 Wind, Wave, Stress, and Surface Roughness Relationships from Turbulence Measurements made on R/P FLIP in the SCOPE Experiment," *NOAA Technical Memorandum ERL ETL-268*, 1996.

[5] W. M. Drennan, H. C. Graber, D. Hauser, and C. Quentin, "On the wave age dependence of wind stress over pure wind seas," *Journal of Geophysical Research*, vol. 108, no. C3, p. 8062, mar 2003. [Online]. Available: http://doi.wiley.com/10.1029/2000JC000715

[6] J. MacMahan, "Increased Aerodynamic Roughness Owing to Surfzone Foam," *Journal of Physical Oceanography*, vol. 47, no. 8, pp. 2115–2122, aug 2017. [Online]. Available: http://journals.ametsoc.org/doi/10.1175/JPO-D-17-0054.1

[7] P. A. Jiménez and J. Dudhia, "On the Need to Modify the Sea Surface Roughness Formulation over Shallow Waters," *Journal of Applied Meteorology and Climatology*, vol. 57, no. 5, pp. 1101–1110, may 2018. [Online]. Available: http://journals.ametsoc.org/doi/10.1175/JAMC-D-17-0137.1

[8] N. National Geophysical Data Center, "U.S. Coastal Relief Model - Southern California," 2016.

[9] N. J. M. Laxague, M. Curcic, J.-V. Bjorkqvist, and B. K. Haus, "Gravity-Capillary Wave Spectral Modulation by Gravity Waves," *IEEE Transactions on Geoscience and Remote Sensing*, vol. 55, no. 5, pp. 2477–2485, may 2017. [Online]. Available: http://ieeexplore.ieee.org/document/7828133/

[10] J. Apel and F. Gonzalez, "Nonlinear features of internal waves off Baja California as observed from the SEASAT imaging radar," *Journal of Geophysical Research*, vol. 88, no. C7, p. 4459, 1983. [Online]. Available: http://doi.wiley.com/10.1029/JC088iC07p04459

[11] O. Phillips, *The Dynamics of the Upper Ocean*, 2nd ed. Cambridge: Cambridge University Press, 1980.

[12] R. S. Dietz and E. C. Lafond, "Natural Slicks on the Ocean," *Journal of Marine Research*, 1950. [Online]. Available: http://www.dtic.mil/docs/citations/ADA314074

[13] G. C. Ewing, "Relation between Band Slicks at the Surface and Internal Waves in the Sea," *Source: Science, New Series*, vol. 111, no. 2874, pp. 91–94, 1950. [Online]. Available: http://www.jstor.org/stable/1677172 http://about.jstor.org/terms

[14] P. Brandt, R. Romeiser, and A. Rubino, "On the determination of characteristics of the interior ocean dynamics from radar signatures of internal solitary waves," *Journal of Geophysical Research: Oceans*, vol. 104, no. C12, pp. 30 039–30 045, dec 1999. [Online]. Available: http://doi.wiley.com/10.1029/1999JC900092

[15] M.-K. Hsu and A. Liu, "Nonlinear Internal Waves in the South China Sea," *Canadian Journal of Remote Sensing*, vol. 26, no. 2, 2000.

[16] J. A. MacKinnon and M. C. Gregg, "Spring Mixing: Turbulence and Internal Waves during Restratification on the New England Shelf," *Journal of Physical Oceanography*, vol. 35, no. 12, pp. 2425–2443, dec 2005. [Online]. Available: http://journals.ametsoc.org/doi/abs/10.1175/JPO2821.1

[17] S. H. Wong, A. E. Santoro, N. J. Nidzieko, J. L. Hench, and A. B. Boehm, "Coupled physical, chemical, and microbiological measurements suggest a connection between internal waves and surf zone water quality in the Southern California Bight," *Continental Shelf Research*, vol. 34, pp. 64–78, feb 2012. [Online]. Available: https://www.sciencedirect.com/science/article/pii/S0278434311003761

[18] A. Monin and A. Oboukhov, "Basic Laws of Turbulent Mixing in the Surface Layer of the Atmosphere," *Tr. Akad Nauk SSSR Geophiz*, vol. 24, no. 151, p. 30, 1954.

[19] U. Högström, A. Rutgersson, E. Sahlée, A.-S. Smedman, T. S. Hristov, W. M. Drennan, and K. K. Kahma, "Air-Sea Interaction Features in the Baltic Sea and at a Pacific Trade-Wind Site: An Inter-comparison Study," *Quarterly Journal of the Royal Meteorological SocietyBoundary-Layer Meteorology*, vol. 147, no. 1, pp. 139–163, apr 2013. [Online]. Available: http://link.springer.com/10.1007/s10546-012-9776-8

[20] A. A. Grachev, L. S. Leo, H. J. S. Fernando, C. W. Fairall, E. Creegan, B. W. Blomquist, A. J. Christman, and C. M. Hocut, "Air-Sea/Land Interaction in the Coastal Zone," *Boundary-Layer Meteorology*, vol. 167, no. 2, pp. 181–210, dec 2018. [Online]. Available: http://link.springer.com/10.1007/s10546-017-0326-2

[21] Q. Wang, D. P. Alappattu, S. Billingsley, B. Blomquist, R. J. Burkholder, A. J. Christman, E. D. Creegan, T. de Paolo, D. P. Eleuterio, H. J. S. Fernando, K. B. Franklin, A. A. Grachev, T. Haack, T. R. Hanley, C. M. Hocut, T. R. Holt, K. Horgan, H. H. Jonsson, R. A. Hale, J. A. Kalogiros, D. Khelif, L. S. Leo, R. J. Lind, I. Lozovatsky, J. Panella-Morato, S. Mukherjee, W. A. Nuss, J. Pozderac, L. T. Rogers, I. Savelyev, D. K. Savidge, R. K. Shearman, L. Shen, E. Terrill, A. M. Ulate, Q. Wang, R. T. Wendt, R. Wiss, R. K. Woods, L. Xu, R. T. Yamaguchi, and C. Yardim, "CASPER: Coupled Air-Sea Processes and Electromagnetic (EM) ducting Research," *Bulletin of the American Meteorological Society*, pp. BAMS–D–16–0046.1, nov 2017. [Online]. Available: http://journals.ametsoc.org/doi/10.1175/BAMS-D-16-0046.1

[22] D. G. Ortiz-Suslow, J. Kalogiros, R. Yamaguchi, D. Alappattu, K. Franklin, B. Wauer, and Q. Wang, "The Data Processing and Quality Control of the Marine Atmospheric Boundary Layer Measurement Systems Deployed by the Naval Postgraduate School during the CASPER-West Field Campaign," Naval Postgraduate School, Monterey, Tech. Rep., 2019. [Online]. Available: http://hdl.handle.net/10945/61638

[23] J. C. McWilliams, F. Colas, and M. J. Molemaker, "Cold filamentary intensification and oceanic surface convergence lines," *Geophysical Research Letters*, vol. 36, no. 18, p. L18602, sep 2009. [Online]. Available: http://doi.wiley.com/10.1029/2009GL039402